Human Molecular Genetics, 2011, Vol. 20, No. 23 ***4530–4539***
doi:10.1093/hmg/ddr394
Advance Access published on September 7, 2011

Modeling familial Alzheimer's disease with induced pluripotent stem cells

Takuya Yagi[1], Daisuke Ito[1,*], Yohei Okada[2,3], Wado Akamatsu[2], Yoshihiro Nihei[1], Takahito Yoshizaki[1], Shinya Yamanaka[4], Hideyuki Okano[2] and Norihiro Suzuki[1]

[1]Department of Neurology, [2]Departments of Physiology and [3]Kanrinmaru Project, School of Medicine, Keio University, 35 Shinanomachi, Shinjuku-ku, Tokyo 160-8582, Japan and [4]Center for iPS Cell Research and Application, Kyoto University, Kyoto 606-8507, Japan

Received June 3, 2011; Revised August 1, 2011; Accepted August 29, 2011

Alzheimer's disease (AD) is the most common form of age-related dementia, characterized by progressive memory loss and cognitive disturbance. Mutations of presenilin 1 (*PS1*) and presenilin 2 (*PS2*) are causative factors for autosomal-dominant early-onset familial AD (FAD). Induced pluripotent stem cell (iPSC) technology can be used to model human disorders and provide novel opportunities to study cellular mechanisms and establish therapeutic strategies against various diseases, including neurodegenerative diseases. Here we generate iPSCs from fibroblasts of FAD patients with mutations in *PS1* (A246E) and *PS2* (N141I), and characterize the differentiation of these cells into neurons. We find that FAD–iPSC-derived differentiated neurons have increased amyloid β42 secretion, recapitulating the molecular pathogenesis of mutant presenilins. Furthermore, secretion of amyloid β42 from these neurons sharply responds to γ-secretase inhibitors and modulators, indicating the potential for identification and validation of candidate drugs. Our findings demonstrate that the FAD-iPSC-derived neuron is a valid model of AD and provides an innovative strategy for the study of age-related neurodegenerative diseases.

INTRODUCTION

Alzheimer's disease (AD) is one of the most common neurodegenerative disorders of the elderly, characterized by progressive memory disorientation and cognitive disturbance. The pathological profile of AD is neuronal loss in the cerebral cortex accompanied by massive accumulation of two types of amyloid fibril seeding senile plaques and hyperphosphorylated tau forming paired helical filaments. The amyloid fibril is mainly composed of β-amyloid (Aβ) peptides, the 40 and 42 amino acid forms (Aβ40 and Aβ42), that are derived by proteolytic cleavages from the amyloid precursor protein (APP) by β- and γ-secretase activity (1,2). According to the amyloid cascade hypothesis, a prevailing theory of AD pathology, accumulation of Aβ, mainly Aβ42, in the brain is the initiator of AD pathogenesis, subsequently leading to the formation of neurofibrillary tangles containing hyperphosphorylated tau protein, and consequently neuronal loss (3–5).

Presenilin 1 (*PS1*) and presenilin 2 (*PS2*) genes encoding the major component of γ-secretase have been identified as the causative genes for autosomal-dominant familial Alzheimer's disease (FAD). Mutations in the *PS1* gene, located on chromosome 14, occur most frequently in FAD (6,7). Ala246Glu (A246E) in *PS1* is a well-characterized FAD mutation that shows typical phenotypes of AD with complete penetrance. Mutations in the *PS2* gene on chromosome 1 are a relatively rare cause of FAD and are variably penetrant. Asn-141 substitutions by Ile (N141I) in the *PS2* gene was the first identified causative mutation of *PS2* in affected patients from the now famous Volga German families (8,9).

Mutations in the *PS1*, *PS2* and the *APP* gene account for most of the familial early onset cases of AD either by enhancing the production of pathological Aβ or especially Aβ42, which has a greater tendency to form fibrillary amyloid deposits. These findings support β-amyloid as the common initiating factor in AD in the amyloid cascade hypothesis (10,11). Both A246E in *PS1* and N141I in *PS2* are reported to induce

*To whom correspondence should be addressed at: Department of Neurology, School of Medicine, Keio University, 35 Shinanomachi, Shinjuku-ku, Tokyo 160-8582, Japan. Tel: +81 353633788; Fax: +81 333531272; Email: d-ito@jk9.so-net.ne.jp

elevation of Aβ42 levels in human plasma, patient-derived fibroblasts, forced-expressed cells and, in mice, showing strong toxicity (10–13).

Generation of human iPSCs provides a new method for elucidating the molecular basis of human disease (14,15). An increasing number of studies have employed disease-specific human iPSCs in neurological diseases, and a few have demonstrated disease-specific phenotypes to model the neurological phenotype (16–24). Here, we report the generation of iPSC from fibroblasts of FAD with the *PS1* mutation A246E and the *PS2* mutation N141I, and differentiation of these cells into neurons. We demonstrate that patient-derived differentiated neurons increase Aβ42 secretion, recapitulating the pathological mechanism of FAD with *PS1* and *PS2* mutations. Our findings demonstrate that the FAD–iPSC-derived neuron is a valid model for studying AD, and provides important clues for the identification and validation of candidate drugs.

RESULTS

Generation of iPSC with presenilin mutations

We established two clones of iPSCs with the *PS1* mutation, A246E (PS1-2 iPSC and PS1-4 iPSC) and with the *PS2* mutation, N141I (PS2-1 iPSC and PS2-2 iPSC) by retroviral transduction of primary human fibroblasts with the five factors OCT4, SOX2, KLF4, LIN28 and NANOG. Fibroblasts were obtained from the Coriell Cell Repository (AG07768 and AG09908). The 201B7 iPSC line (14) and the sporadic Parkinson disease (PD)-derived iPSC lines (PD01-25 and 26) were reprogrammed by an original method (14) with four transcription factors (OCT4, SOX2, KLF4 and cMYC) and were used as the controls in this study. Genotyping of the established iPSC lines was confirmed by PCR–RFLP and sequencing (Fig. 1A and B). All PS1 and PS2 iPSC clones demonstrated typical characteristics of pluripotent stem cells: similar morphology to ESCs, expression of pluripotent markers including Tra-1-60, Tra-1-81, SSEA3 and SSEA4 (Fig. 1C), silencing of retroviral transgenes and reactivation of genes indicative of pluripotency (Fig. 1D). The differentiation ability of PS1 and PS2 iPSC was also confirmed *in vivo* by teratoma formation (Fig. 2), and *in vitro* by the formation of three germ layers via embryoid bodies (Supplementary Material, Fig. S1). To validate our reprogramming technique, we performed comprehensive analysis of two PS2 iPSCs. Heat map analysis showed that global gene expression profiles, including the critical genes for pluripotency, were similar between the iPSC lines established with four transcription factors (201B7 and PD01-25) and the PS2 iPSC clones established with five transcription factors (Supplementary Material, Fig. S2). In addition, there were no significant differences in the expression of AD-related molecules between PS2 iPSCs and control iPSCs (Supplementary Material, Fig. S3). Array comparative genomic hybridization (aCGH) analysis on PS2-1, PS2-2 iPSC and AG09908 fibroblasts showed that the total number of copy number aberrations were 52, 61 and 102 out of ∼17 000 locations, respectively (Supplementary Material, Table S1), and no aberrations were detected in *APP*, *PS1* and *PS2* genes.

Differentiation of PS1 iPSC and PS2 iPSC into neurons

Differentiation of FAD patient-specific iPSCs towards neurons enables modeling the disease pathogenesis *in vitro*. To establish whether the presenilin mutations may affect neuronal differentiation, both PS1 and PS2 iPSC lines, as well as control iPSC lines, were induced to differentiate into neural cells (25,26), and cultured on Matrigel-coated dishes for 2 weeks to induce terminal differentiation (Fig. 3). We confirmed neuronal differentiation by the expression of neuronal markers, βIII-tubulin, and MAP-2 (Fig. 3A and B). As shown in Figure 3C, no obvious differences in the ability to generate neurons (∼80% βIII-tubulin-positive cells) were observed among control, PS1 and PS2 iPSCs. This indicated that PS1 and PS2 iPSCs can generate neurons with almost the same efficiency as the control iPSCs, suggesting these presenilin mutations may have no significant effect on neuronal differentiation.

Production of Aβ secreted from iPSCs-derived neurons

To analyze the functional aspects of FAD, we investigated Aβ secretion from iPSC or iPSC-derived neurons. The Aβ secretion in the conditioned medium from control iPSC, PS1 iPSC and PS2 iPSC was very low; Aβ42 secretion especially was below the detection sensitivity. We therefore could not compare the ratio of Aβ42 to Aβ40 among iPSC lines. However, the Aβ secretion in the conditioned medium from the iPSCs-derived neurons was increased and measurable, indicating that Aβ secretion could undergo significant fluctuation during differentiation. Although the levels of Aβ42 and Aβ40 in the medium showed some clonal variation (Fig. 4A), possibly depending on the rate of cell growth and passage number, the ratio of Aβ42 to Aβ40 was significantly elevated in the PS1 and PS2 iPSCs-derived neurons, compared with the controls (Fig. 4B). Thus, PS1 and PS2 iPSCs show that living neurons derived from patients with the presenilin mutations ending at residue 42 that are linked to FAD secrete more Aβ. This result is compatible with previous evidences based on patients' plasma, fibroblasts and forced-expressed cells (10–13).

To explore recapitulation of key pathological events in AD, we investigated whether FAD-iPSC-derived differentiated neurons exhibit abnormal accumulation of tau and performed an immunoblot analysis of lysates of FAD-iPSC-derived neurons with anti-tau antibody. However, as shown in Supplementary Material, Figure S4, no abnormal tau protein accumulation or tangle formation was detected in the FAD-derived neurons, indicating that recapitulation of tauopathy is difficult to observe during the short culture period (2 weeks) in the present protocol.

Pharmacological response to γ-secretase inhibitors in PS1 iPSC- and PS2 iPSC-derived neurons

To evaluate the capacity of pharmacological drug screening in iPSC technology, we assessed whether inhibitors could affect the secretion of Aβ in PS1 and PS2 iPSCs-derived neurons. We first examined the secretion of Aβ from PS1-4 and PS2-2 iPSCs-derived neurons in the presence of Compound E, a

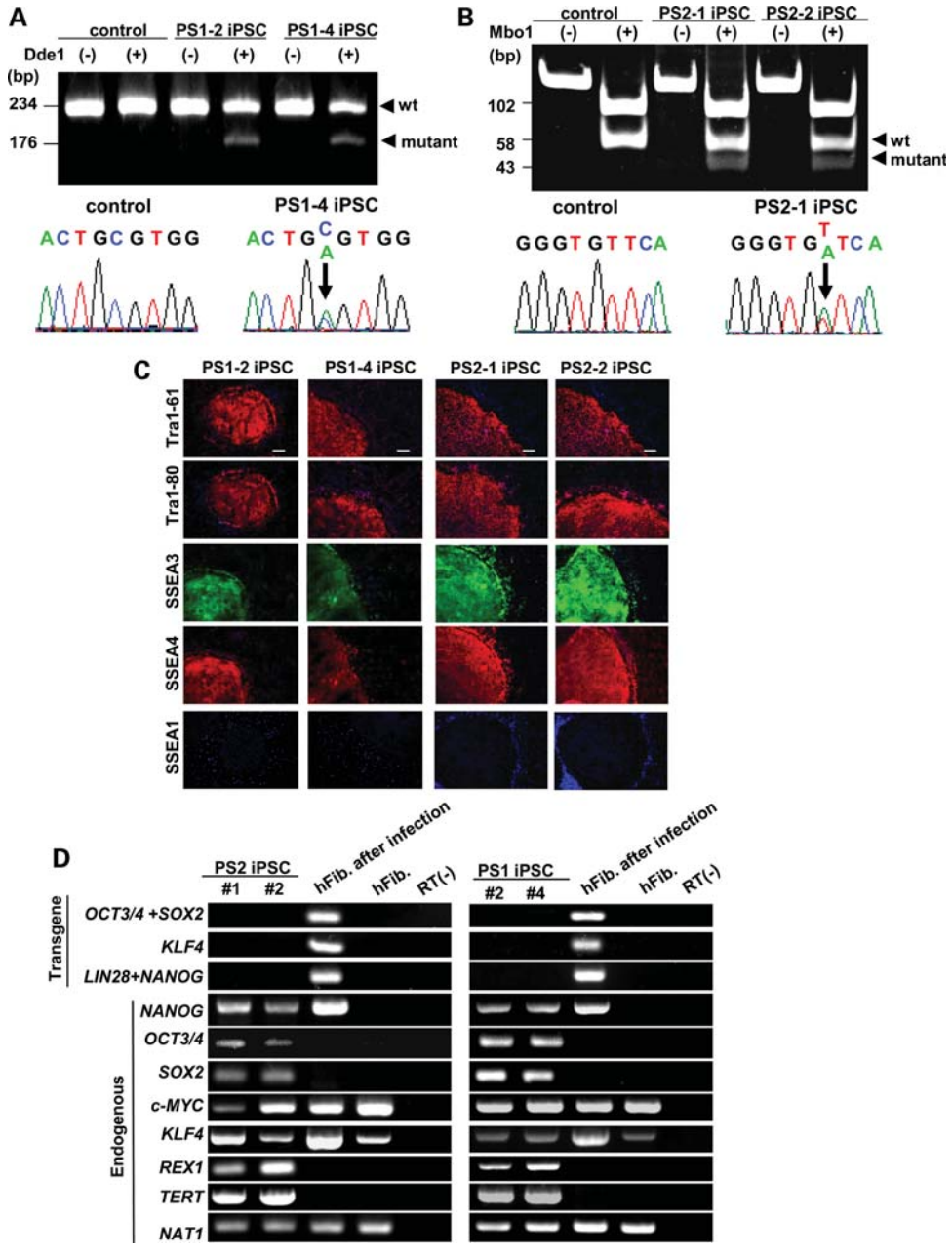

Figure 1. Generation of PS1 and PS2 iPSC from patient fibroblasts. (**A**) Genotypic analysis of PS1 iPSC by PCR–RFLP and sequencing. A246E genotyping by PCR–RFLP was performed with restriction enzyme *Dde*I. The A246E mutation results in fragments of 176 and 58 bp, whereas the control fragment has 234 bp. (**B**) Genotypic analysis of PS2 iPSC by PCR–RFLP and sequencing. N141I genotyping by PCR–RFLP was performed with restriction enzyme *Mbo*I. The N141I mutation results in fragments of 102, 58 and 43 bp, whereas the control has fragment lengths of 102 and 58 bp. (**C**) Both PS1 and PS2 iPSC lines exhibit markers of pluripotency. All iPSCs express pluripotency markers including Tra-1-60, Tra-1-81, SSEA3 and SSEA4. Nuclei were stained with 4,6-diamidino-2-phenylindole (DAPI). Bar = 200 μm. (**D**) RT–PCR analysis of the transgenes OCT3/4, SOX2, KLF4 and the endogenous hESC marker genes. Patient fibroblasts 6 days after the transduction with the retroviruses are positive for the transgenes.

potent γ-secretase inhibitor (27) (Fig. 5A and B). With the addition of 10 and 100 nM Compound E, the production of both Aβ42 and Aβ40 was suppressed in a dose-dependent manner, when compared with untreated in both of PS1-4 and PS2-2 iPSC-derived neurons. Next, we assessed the ability of Compound W, a selective Aβ42-lowering agent, to modulate γ-secretase-mediated APP cleavage (28) (Fig. 5A and B). As expected, the addition of Compound W caused a drastic decrease in the ratio of Aβ42 to Aβ40 in both neurons.

We also determined the effect of these compounds on the proteolytic processing that causes a release of an intracellular domain of Notch, another γ-secretase substrate. Western blotting using the anti-S3 cleaved Notch1-specific antibody demonstrated that productions of Notch intracellular domain

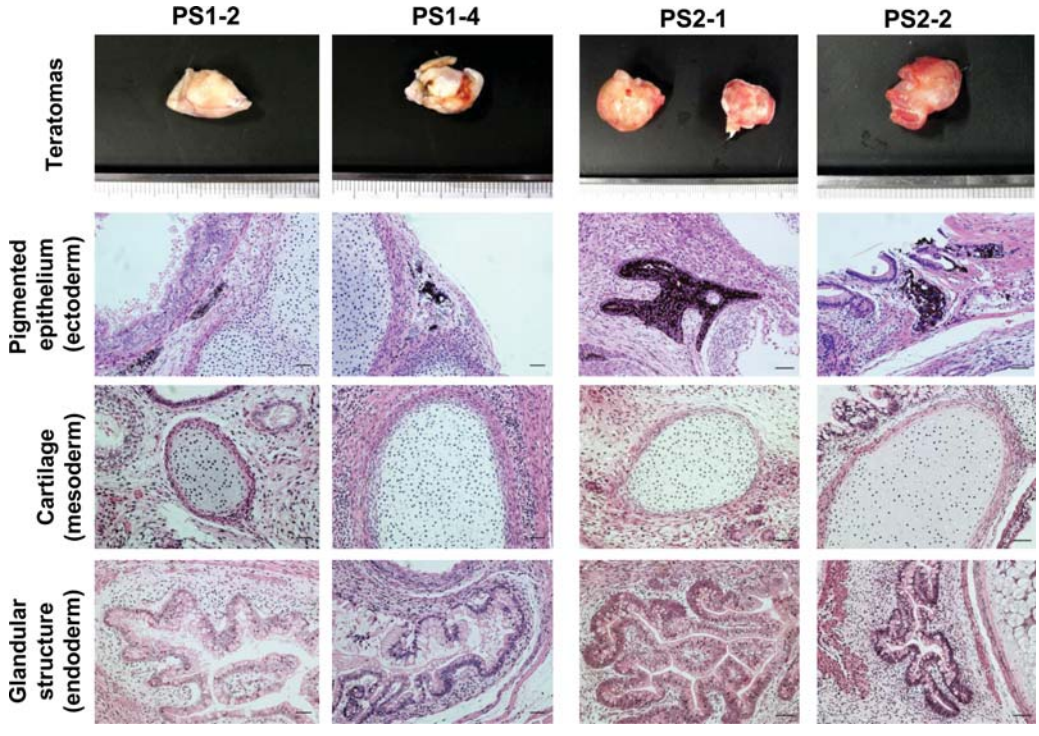

Figure 2. Teratomas derived from SCID mice injected with PS1 and PS2 iPSCs. Gross morphology, hematoxylin and eosin stained representative teratoma generated from PS 1 (PS1-2 iPSC and PS1-4 iPSC) and PS2-1 iPSC (PS2-1 iPSC and PS2-2 iPSC). Both iPSC shows tissues representing all three embryonic germ layers, including pigmented epithelium (ectoderm), cartilage (mesoderm) and glandular structure (endoderm). Bar = 50 μm.

(NICD) from both PS1-4 and PS2-2 iPSCs-derived neurons exposed to Compound E was inhibited in a dose-dependent manner. Although high dose (100 μM) of Compound W seemed to decrease NICD production in PS1-4, both neurons exposed to Compound W showed that NICD was mostly maintained (Fig. 5C). Taken together, these data indicate that both PS1 and PS2 iPSC-derived neurons respond to drug treatment in an expected manner and might be useful for drug screening in AD.

DISCUSSION

To the best of our knowledge, this study is the first to demonstrate a model of FAD using the iPSC technology. Using human neurons carrying a *PS1* mutation and a *PS2* mutation, we observed an elevation of the ratio of Aβ42 to Aβ40, a hallmark feature of FAD with presenilin mutations, in neurons derived from two clones of PS1 and PS2 iPSCs, when compared with non-AD controls (201B7, PD01-25 and 26) (Fig. 4). Although an increase in Aβ42 levels as a result of the A246E mutation in *PS1* and N141I mutation in *PS2* has been reported in patient-derived fibroblasts (11), the present study provided the first evidence of increased Aβ42 secretion by living human neurons derived from AD patients, thereby directly supporting the amyloid cascade hypothesis. To test the possibility of using the iPSC technology for drug screening, we checked the pharmacological responses to a known γ-secretase inhibitor and modulator (Fig. 5A and B). Results showed that Aβ secretion by adding agents against γ-secretase were inhibited or modulated as expected. Moreover, the Notch signaling pathway reacted with proteolytic cleavage in the presence of γ-secretase inhibitors (Fig. 5C). Recent studies have revealed that γ secretase activity is influenced in a complex manner by several cellular factors, including rafts, trafficking, expression levels of CD147, numb and gamma-secretase activating protein (1,2,29–31). We therefore propose that living human neurons from patients, i.e. FAD-iPSC-derived neurons, are very suitable material for drug development and validation of new drugs.

Previous studies on patient-specific iPSC models have mostly been limited to genetic congenital disorders (19,20,22,24,32–35). Congenital disorders may be suitable for modeling disease-specific phenotypes in the iPSC technology, because differentiated cells generated from iPSC could represent the developmental stages of disease (36). However, modeling familial PD using iPSC that carry the p.G2019S mutation in the Leucine-Rich Repeat Kinase-2 (LRRK2) gene has been reported recently (23). DA neurons derived from G2019S-iPSCs were vulnerable to exposure to stress agents, such as hydrogen peroxide, MG-132 and 6-hydroxydopamine. Now we also demonstrate the possibility of modeling the most common aging-related neurodegenerative disorder, AD, by recapitulating the key pathological mechanism (Fig. 4). Many insights into the molecular pathogenesis in neurodegenerative diseases have come from investigating post-mortem brain tissues or transgenic animals, due to the difficulty of invasive access to the living human central nervous system. With disease modeling using the iPSC technology, these new tools will make it possible to analyze living disease-specific

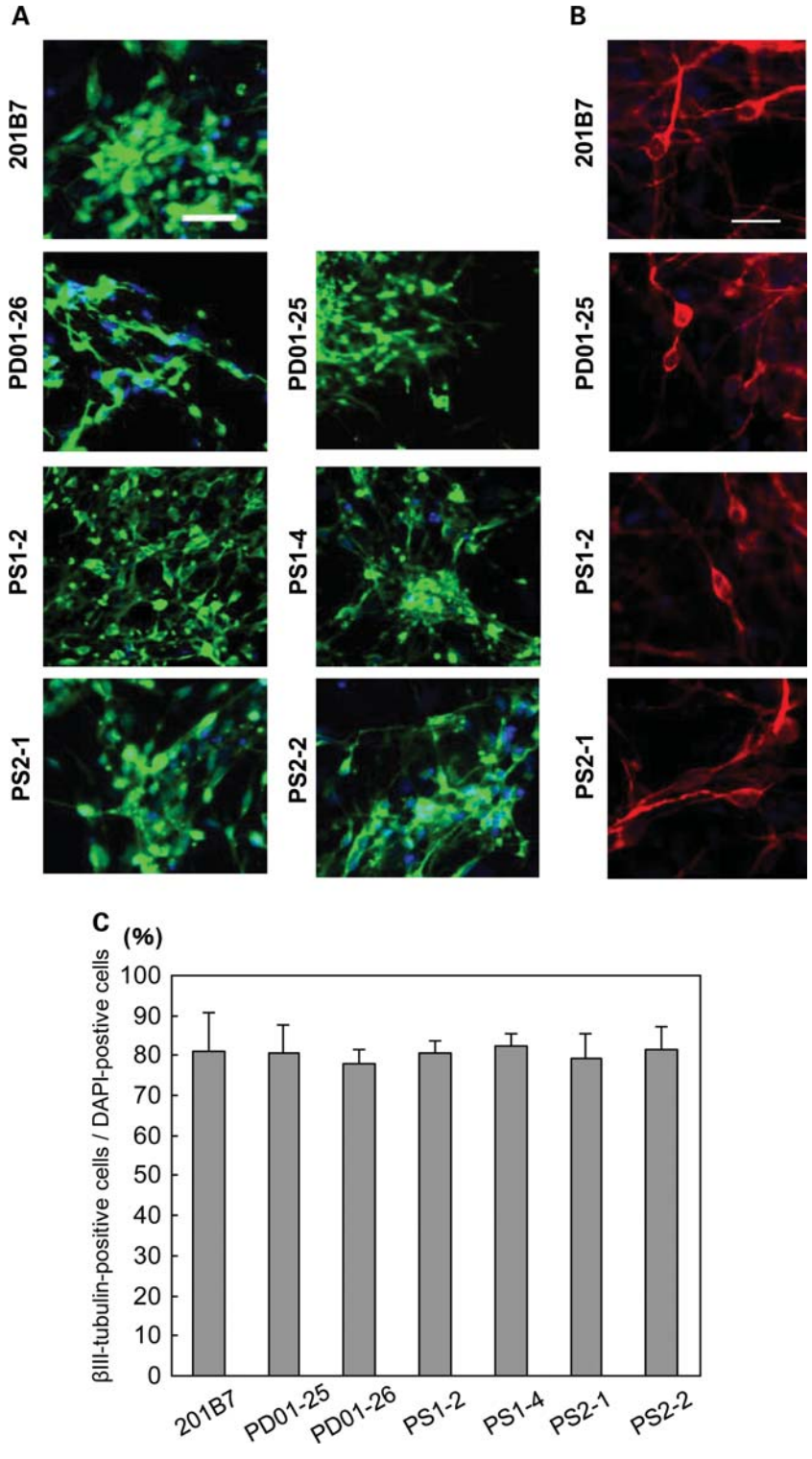

Figure 3. Differentiation of PS1 and PS2 iPSC into neurons. (**A** and **B**) Neural differentiation of control iPSC (201B7, PD01-25 and PD01-26), PS1 iPSC (PS1-2 iPSC and PS1-4 iPSC) and PS2 iPSC (PS2-1 iPSC and PS2-2 iPSC). Representative pictures of immunocytochemistry for βIII-tubulin (A) and MAP-2 (B) after neural differentiation. Bar = 40 μm (A) and 20 μm (B). (**C**) Graphs indicate the percentage of βIII-tubulin-positive cells relative to cells with DAPI-staining nuclei. Error bars indicate the SD ($n = 3$).

neurons *in vitro*. Moreover, we could graft disease-specific neurons derived from iPSCs into the brain of immunodeficient animals and we could investigate the time-dependent pathological changes *in vivo* in future studies.

FAD iPSCs could be a potential strategy for drug discovery against AD as described here; however, several limitations must be addressed in future studies. First, a high-yield of differentiated neurons from human iPSCs requires multistep

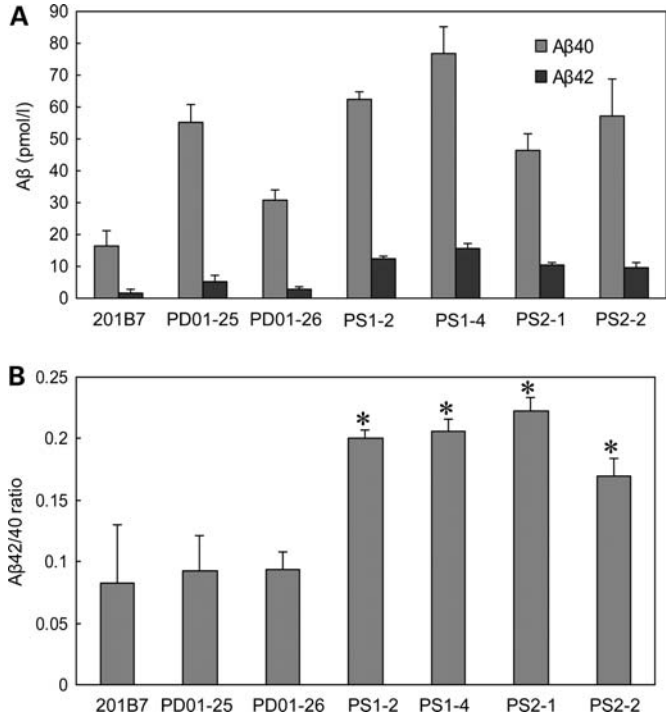

Figure 4. Characterization of Aβ secretion in PS1 and PS2 iPSC-derived neurons. (**A**) The amount of Aβ40 and Aβ42 secreted from control iPSC-derived neurons, PS1 iPSC (PS1-2 iPSC and PS1-4 iPSC) and PS2 iPSC (PS2-1 iPSC and PS2-2 iPSC)-derived neurons. (**B**) The ratio of Aβ42/Aβ40 from control iPSC-derived neurons, PS1 iPSC-derived neurons and PS2 iPSC-derived neurons. Note, the ratio of Aβ42/Aβ40 in both PS1 iPSC-derived neurons and PS2 iPSC-derived neurons was significantly higher than that of control iPSC-derived neurons. Significant differences among groups were examined by Student's *t*-test versus the ratio of 201B7 iPSC-derived neurons ($^*P < 0.05$).

procedures and prolonged culture. Furthermore, heterogeneity of differentiated neuronal cell types depending on clonal variability and culture conditions is inevitable using current differentiation methods. Clonal variation in their characters, including differentiation efficiency and tumor formation, has been a problem that needed to be solved thus far (26,37,38). Development of reliable protocols for more rapid neuronal differentiation with minimal clonal variation will be necessary, if drug discovery using iPSCs is to be fruitful. Secondly, another defining pathology in AD is an accumulation of hyperphosphorylated tau forming paired helical filaments. Growing evidence reveals that toxic Aβ directly induces tau hyperphosphorylation and accumulation, leading to neurodegeneration processes in affected neurons in AD (39,40). Pathological observations reveal that tau aggregates, but not amyloid deposits, actually correlate with dementia severity and extent of neuronal loss (41,42). Therefore, whether FAD iPSC-derived neurons exhibit accumulation of phosphorylated tau during extended culture periods should be addressed, and future studies must also focus on the biochemical dynamics of tau protein in iPSC-derived neurons treated with exogenous Aβ. Thirdly, the pathological mechanism of late-onset AD, sporadic AD and AD harboring the apoE4 allele remains unclear. Recent studies propose that impaired clearance of Aβ may cause late-onset AD through interactions with ApoE4, rather than increased Aβ production (43,44). Late-onset AD is more common and accounts for 90% of people suffering with Alzheimer's disease. To establish therapeutic strategies targeting the common form of AD, neurons derived from patient-specific iPSCs should be applied to investigations into the mechanisms underlying Aβ clearance.

Recently, a number of clinical trials of drugs targeting the pathogenesis of AD have reportedly failed in succession. Although future advances in iPSC methods are necessary for the pharmacological development and clinical application of iPSCs in neurodegeneration, we hope that our study will contribute significantly towards the identification and validation of novel candidate drugs against one of the most common and intractable diseases, AD.

MATERIALS AND METHODS

Cell culture and iPS generation

PS1 A246E fibroblasts (AG07768) and *PS2* N141I fibroblasts (AG09908) were obtained from Coriell Cell Repository. Human fibroblasts were cultured in Dulbecco's Modified Eagle's Medium (DMEM; Gibco) containing 10% fetal bovine serum, 50 U/ml penicillin, 50 mg/ml streptomycin and 1 mM L-glutamine. PS1 iPSC and PS2 iPSC were generated using the Human iPS Cell Generation Vector Set (TAKARA). G3T-hi cells were transfected with the Human iPS Cell Generation Vector set (pDON-5 OCT3/4-SOX2, pDON-5 KLF4, pDON-5 LIN28-NANOG) and pGP Vector and pE-ampho Vector with TransIT-293. Forty-eight hours after transfection, the medium (virus-containing supernatant) was collected and filtered through a 0.45 mM pore-size cellulose acetate filter. Next, the retrovirus-containing supernatant was added to RetroNectin-coated plates for centrifugation at 32°C and 2000*g* for 2 h to facilitate attachment of the virus particles onto the RetroNectin. Following this, fibroblasts were added to the plate and retrovirally transduced. Six days after transduction, fibroblasts were harvested by trypsinization and replated at 1×10^5 cells per 100 mM dish on mitomycin C-inactivated SNL cells, and the medium was changed to hiPSC medium, which consisted of DMEM/F12 medium (Invitrogen) supplemented with 20% Knock-out Serum Replacement (Invitrogen), 1 mM L-glutamine, 1 mM non-essential amino acids, 0.1 mM β-mercaptoethanol, 50 U penicillin, 50 mg/ml streptomycin (Invitrogen) and 4 ng/ml basic fibroblast growth factor (bFGF; WAKO Pure Chemicals). The hiPSC medium was changed every other day until colonies were picked. The generated iPSCs were maintained on mitomycin C-inactivated SNL cells. The hiPSC-culture medium was changed every other day, and the cells were passaged using CTK solution every 6–7 days.

Sporadic PD patient fibroblasts were generated from dermal biopsies following informed consent under protocols approved by Keio University. Two neurologists diagnosed the patient with sporadic PD, AD was excluded. Sporadic PD-derived iPSCs were generated as reported previously (14).

Reverse transcriptase-polymerase chain reaction

Total RNA samples were isolated using RNeasy (Qiagen), according to the manufacturer's instructions. The concentration

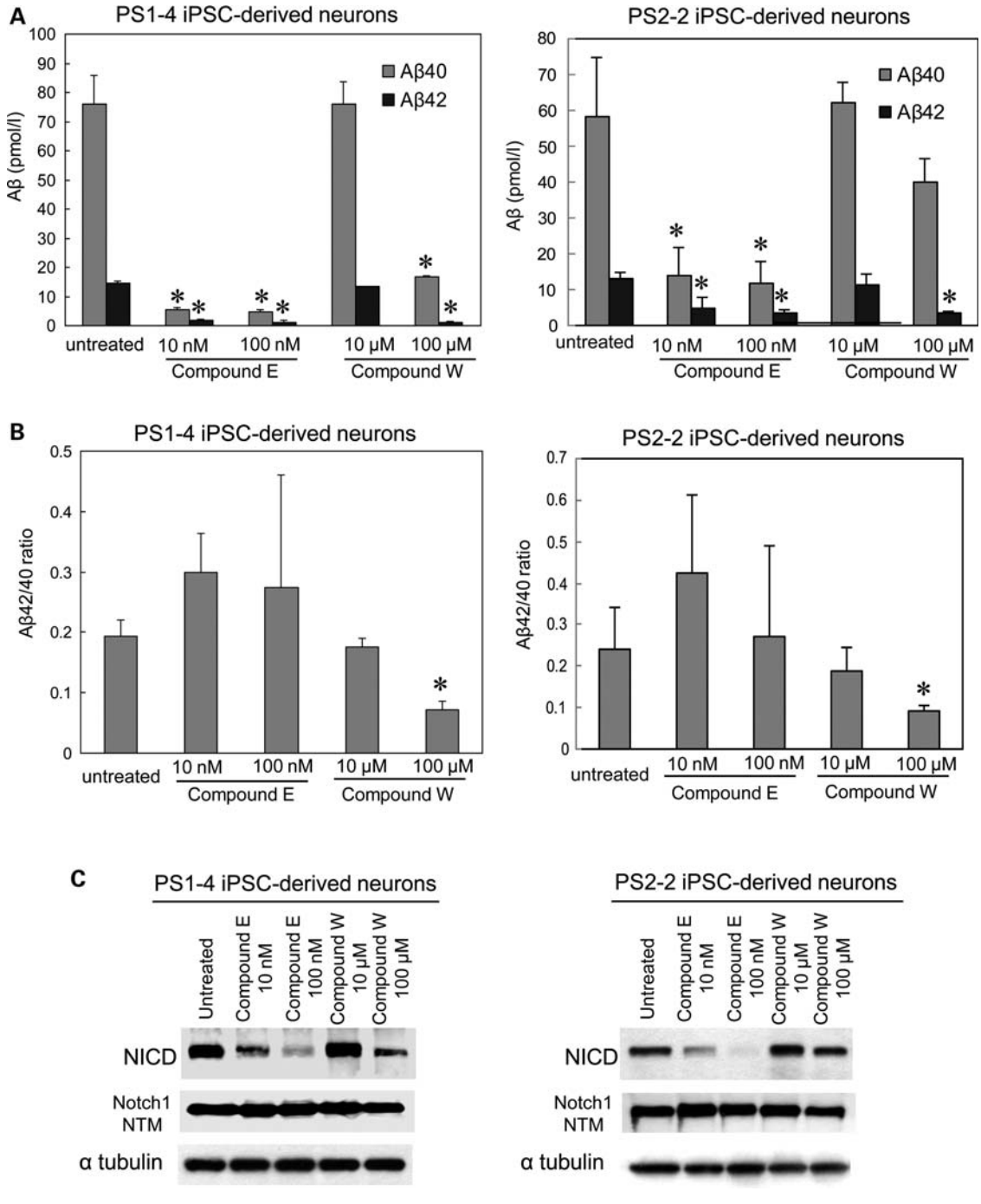

Figure 5. Pharmacological response to γ-secretase inhibitors in PS1 and PS2 iPSC-derived neurons. (**A**) The amount of Aβ40 and Aβ42 secreted from PS1-4 iPSC-derived neurons (left graph) and PS2-2 iPSC-derived neurons (right graph) treated with Compound E or W. Significant differences were examined by Student's *t*-test versus Aβ40 or Aβ42 of untreated, respectively (*$P < 0.05$). (**B**) The ratio of Aβ42/Aβ40 from PS1-4 iPSC-derived neurons (left) and PS2-2 iPSC-derived neurons (right). Significant differences were examined by Student's *t*-test versus the ratio of untreated (*$P < 0.05$). (**C**) Western blotting of S3 cleaved NICD (∼110 kDa) and uncleaved Notch1 transmembrane subunit (∼120 kDa) in PS1-4 iPSC-derived neurons (left) and PS2-2 iPSC-derived neurons (right) exposed to Compound E or W. α-Tubulin served as internal loading controls. Error bars in (A–D) indicate SD from three independent experiments.

and purity of the RNA was determined using the ND-1000 spectrophotometer (Nanodrop). The cDNA was synthesized using the SuperscriptIII First-Strand Synthesis System (Invitrogen). The transgene primers used in the PCR are listed in Supplementary Material, Table S2. The endogenous primers have been described previously (14).

Immunofluorescence staining of iPS and iPSC-derived differentiated neurons

Immunofluorescence staining was performed using the following primary antibodies: anti-SSEA 3 (Abcam), anti-SSEA 4 (Abcam), anti-Tra-1-60 (Millipore), anti-Tra-1-81 (Millipore),

anti-SSEA1 (Abcam), anti- MAP-2 (Chemicon) and anti-tau (HT7, Thermoscientific). 4,6-Diamidino-2-phenylindole (DAPI; Molecular Probes) was used for nuclear staining. The secondary antibodies used were: anti-rat IgG and anti-mouse IgG, and IgM conjugated with Alexa Fluor 488 or Alexa Fluor 568 (Molecular Probes).

Microarray analysis

Human genome U133 Plus 2.0 GeneChip arrays carrying 54 690 probe sets (Affymetrix) were used for microarray hybridizations to examine global gene expression. Approximately 150 ng of RNA from each sample was labeled using GeneChip 3′IVT Express (Affymetrix) according to the manufacturer's instructions. All arrays were hybridized at 45°C for 16 h and scanned using an AFX GC3000 G7 scanner. The gene expression raw data were extracted using the AFX Gene Chip Operation System. Quality control was performed on the basis of Affymetrix quality control metrics. The data were analyzed with the Gene Spring GX 11.0 (Agilent). Two normalization procedures were applied. Initially, the signal intensities with values <0.1 were assigned a value of 0.1. Then, each chip was normalized to the 50th percentile of the measurements taken from that chip. Each gene was normalized to the median of that gene in the respective controls, to enable comparisons of relative changes in gene expression levels between different conditions.

Microarray data can be found at the GEO website under accession number 'GSE28379'. (The following link has been created to allow review of record GSE28379: http://www.ncbi.nlm.nih.gov/geo/query/acc.cgi?token=zlovzkaqqwugkdg&acc=GSE28379.) The gene expression profiles of BJ fibroblasts (GSM248214) were downloaded from the NCBI Gene Expression Omnibus (GEO) database.

aCGH analysis

Genomic DNA was isolated using DNeasy (Qiagen), according to the manufacturer's instructions. DNA concentrations were measured on a Nanodrop ND-1000 spectrophotometer (Isogen). DNA quality was monitored with the Agilent 2100 Bioanalyzer (Agilent Technologies). DNA (500 ng) was labeled using the Enzo Genomic DNA Labeling kit. Hybridizations were performed on slides containing four arrays, with each array containing 622 060 *in situ* synthesized 60-mer oligonucleotides, representing 170 344 unique chromosomal locations (Agilent Technologies). Images of the arrays were acquired using a microarray scanner G2505CA (Agilent technologies) and image analysis was performed using feature extraction software version 10.7 (Agilent Technologies). The Agilent CGH-v4_107_Sep09 protocol was applied using default settings. Oligonucleotides were mapped according to the human genome build NCBI 36. The obtained data were imported into Agilent Genomic Workbench using the aberration detection method 2 (ADM-2) algorithm (10.0 threshold) for further analysis. The aCGH data have been deposited in GEO and given the series accession number GSE28450. (The following link has been created to allow review of record GSE28450: http://www.ncbi.nlm.nih.gov/geo/query/acc.cgi?token=ntsvfkqkucksgrc&acc=GSE28450.)

In vitro differentiation

Cells were harvested using CTK solutions and a cell scraper, and transferred to a Petri dish in hiPSC medium without bFGF to form embryoid bodies. After 8 days, embryoid bodies were plated onto gelatin-coated tissue culture dishes and incubated for an additional 8 days. The cells were incubated at 37°C in 5% CO_2 and the medium was replaced every other day. The cells were stained with mouse anti-α-fetoprotein IgG (R&D Systems), anti-smooth muscle actin (Sigma), anti-βIII-tubulin mouse IgG (Chemicon), together with DAPI.

Teratoma formation

hiPSCs were injected into the subcutaneous tissue of SCID mice (CREA). At 8–10 weeks post-injection, teratomas were dissected, fixed in 10% formaldehyde in PBS and embedded in paraffin.

Neural induction

Neural induction of hiPSCs cells was performed as previously described with slight modifications (Okada *et al*., in preparation) (25,26). For terminal differentiation, induced neural cells were plated onto Matrigel-coated coverslips and cultured for 2 weeks. This was followed by the addition of Compound E, 2S-2-{[(3,5-difluorophenyl)acetyl]amino}-*N*-[(3S)-1-methyl-2-oxo-5-phenyl-2,3-dihydro-1H-1,4-benzodiazepin-3-yl]propanamide (Calbiochem) or Compound W, 3,5-Bis(4-nitrophenoxy)benzoic Acid (Tokyo Chemical Industry) for 48 h.

Quantitation of Aβ by ELISA

Conditioned media of differentiated neurons were collected after an incubation period of 48 h and subjected to β Amyloid ELISA Kits (WAKO), according to the manufacturer's instructions.

Immunoblot analysis

Cells were briefly sonicated in cold lysis buffer (50 mM Tris–HCl, pH 7.4, 150 mM NaCl, 0.5% NP-40, 0.5% sodium deoxycholate, 0.25% sodium dodecyl sulfate, 5 mM EDTA and protease inhibitor cocktail from Sigma). Total protein concentration in the supernatant was determined using a Bio-Rad protein assay kit. The proteins were then analyzed by immunoblotting as follows: protein samples were separated by reducing SDS–PAGE on a 4–20% Tris–glycine gradient gel (Invitrogen), and then transferred to a polyvinylidene difluoride membrane (Millipore). The membrane was incubated with primary antibodies and then horseradish peroxidase-conjugated secondary antibodies. Detection was performed using enhanced chemiluminescence reagents as described by the supplier (PerkinElmer Life Sciences). Primary monoclonal antibodies that were used in this study were: anti-tau (HT7, Thermoscientific), anti-NICD (Cell Signaling Technology), anti-Notch1 (D1E11) (Cell Signaling Technology) and alpha tubulin (Cell Signaling Technology).

Statistical analysis

Statistical analysis of the data was performed by Student's *t*-test using JMP 8 (SAS Institute, Inc.).

SUPPLEMENTARY MATERIAL

Supplementary Material is available at *HMG* online.

ACKNOWLEDGEMENTS

T.Y. is a research fellow of the Japan Society for the Promotion of Science. This work was supported by grants from Eisai Co. Ltd (to D.I. and N.S.) and the project for realization of regenerative medicine from the Ministry of Education, Culture, Sports, Science and Technology of Japan to H.O. We thank Mari Fujiwara (Core Instrumentation Facility, Keio University School of Medicine) for the microarray analysis and Satoko Iwasawa (Department of Preventive Medicine and Public Health, School of Medicine, Keio University) for helpful advice about statistical analysis. We also thank Dr Xu Huaxi for providing the T44 Tau pSG5 plasmid (Sanford-Burnham Medical Research Institute).

Conflict of Interest statement. None declared.

FUNDING

This work was supported by grants from Eisai Co. Ltd (to D.I. and N.S.), the Research Fellowship grant of the Japan Society for the Promotion of Science (to T.Y.), and the Project for Realization of Regenerative Medicine, and Support for Core Institutes for iPS Cell Research from the Ministry of Education, Culture, Sports, Science and Technology of Japan (to H.O.).

REFERENCES

1. Vetrivel, K.S. and Thinakaran, G. (2006) Amyloidogenic processing of beta-amyloid precursor protein in intracellular compartments. *Neurology*, **66**, S69–S73.
2. Thinakaran, G. and Koo, E.H. (2008) Amyloid precursor protein trafficking, processing, and function. *J. Biol. Chem.*, **283**, 29615–29619.
3. Hardy, J. and Selkoe, D.J. (2002) The amyloid hypothesis of Alzheimer's disease: progress and problems on the road to therapeutics. *Science*, **297**, 353–356.
4. Tanzi, R.E. and Bertram, L. (2005) Twenty years of the Alzheimer's disease amyloid hypothesis: a genetic perspective. *Cell*, **120**, 545–55.
5. Sisodia, S.S. and St George-Hyslop, P.H. (2002) gamma-Secretase, Notch, Abeta and Alzheimer's disease: where do the presenilins fit in? *Nat. Rev. Neurosci.*, **3**, 281–290.
6. Sherrington, R., Rogaev, E.I., Liang, Y., Rogaeva, E.A., Levesque, G., Ikeda, M., Chi, H., Lin, C., Li, G., Holman, K. *et al.* (1995) Cloning of a gene bearing missense mutations in early-onset familial Alzheimer's disease. *Nature*, **375**, 754–760.
7. Cruts, M., van Duijn, C.M., Backhovens, H., Van den Broeck, M., Wehnert, A., Serneels, S., Sherrington, R., Hutton, M., Hardy, J., St George-Hyslop, P.H. *et al.* (1998) Estimation of the genetic contribution of presenilin-1 and -2 mutations in a population-based study of presenile Alzheimer disease. *Hum. Mol. Genet.*, **7**, 43–51.
8. Levy-Lahad, E., Wasco, W., Poorkaj, P., Romano, D.M., Oshima, J., Pettingell, W.H., Yu, C.E., Jondro, P.D., Schmidt, S.D., Wang, K. *et al.* (1995) Candidate gene for the chromosome 1 familial Alzheimer's disease locus. *Science*, **269**, 973–977.
9. Jayadev, S., Leverenz, J.B., Steinbart, E., Stahl, J., Klunk, W., Yu, C.E. and Bird, T.D. (2010) Alzheimer's disease phenotypes and genotypes associated with mutations in presenilin 2. *Brain*, **133**, 1143–1154.
10. Borchelt, D.R., Thinakaran, G., Eckman, C.B., Lee, M.K., Davenport, F., Ratovitsky, T., Prada, C.M., Kim, G., Seekins, S., Yager, D. *et al.* (1996) Familial Alzheimer's disease-linked Presenilin 1 variants elevate Aβ1-42/1-40 ratio in vitro and in vivo. *Neuron*, **17**, 1005–1013.
11. Scheuner, D., Eckman, C., Jensen, M., Song, X., Citron, M., Suzuki, N., Bird, T.D., Hardy, J., Hutton, M., Kukull, W. *et al.* (1996) Secreted amyloid β-protein similar to that in the senile plaques of Alzheimer's disease is increased in vivo by the presenilin 1 and 2 and APP mutations linked to familial Alzheimer's disease. *Nat. Med.*, **2**, 864–870.
12. Tomita, T., Maruyama, K., Saido, T.C., Kume, H., Shinozaki, K., Tokuhiro, S., Capell, A., Walter, J., Grünberg, J., Haass, C. *et al.* (1997) The presenilin 2 mutation (N141I) linked to familial Alzheimer disease (Volga German families) increases the secretion of amyloid beta protein ending at the 42nd (or 43rd) residue. *Proc. Natl Acad. Sci. USA*, **94**, 2025–2030.
13. Oyama, F., Sawamura, N., Kobayashi, K., Morishima-Kawashima, M., Kuramochi, T., Ito, M., Tomita, T., Maruyama, K., Saido, T.C., Iwatsubo, T. *et al.* (1998) Mutant presenilin 2 transgenic mouse: effect on an age-dependent increase of amyloid beta-protein 42 in the brain. *J. Neurochem.*, **71**, 313–322.
14. Takahashi, K., Tanabe, K., Ohnuki, M., Narita, M., Ichisaka, T., Tomoda, K. and Yamanaka, S. (2007) Induction of pluripotent stem cells from adult human fibroblasts by defined factors. *Cell*, **131**, 861–872.
15. Yu, J., Vodyanik, M.A., Smuga-Otto, K., Antosiewicz-Bourget, J., Frane, J.L., Tian, S., Nie, J., Jonsdottir, G.A., Ruotti, V., Stewart, R. *et al.* (2007) Induced pluripotent stem cell lines derived from human somatic cells. *Science*, **318**, 1917–1920.
16. Dimos, J.T., Rodolfa, K.T., Niakan, K.K., Weisenthal, L.M., Mitsumoto, H., Chung, W., Croft, G.F., Saphier, G., Leibel, R., Goland, R. *et al.* (2008) Induced pluripotent stem cells generated from patients with ALS can be differentiated into motor neurons. *Science*, **321**, 1218–1221.
17. Park, I.H., Arora, N., Huo, H., Maherali, N., Ahfeldt, T., Shimamura, A., Lensch, M.W., Cowan, C., Hochedlinger, K. and Daley, G.Q. (2008) Disease-specific induced pluripotent stem cells. *Cell*, **134**, 877–886.
18. Soldner, F., Hockemeyer, D., Beard, C., Gao, Q., Bell, G.W., Cook, E.G., Hargus, G., Blak, A., Cooper, O., Mitalipova, M. *et al.* (2009) Parkinson's disease patient-derived induced pluripotent stem cells free of viral reprogramming factors. *Cell*, **136**, 964–977.
19. Ebert, A.D., Yu, J., Rose, F.F. Jr., Mattis, V.B., Lorson, C.L., Thomson, J.A. and Svendsen, C.N. (2009) Induced pluripotent stem cells from a spinal muscular atrophy patient. *Nature*, **457**, 277–280.
20. Lee, G., Papapetrou, E.P., Kim, H., Chambers, S.M., Tomishima, M.J., Fasano, C.A., Ganat, Y.M., Menon, J., Shimizu, F., Viale, A. *et al.* (2009) Modelling pathogenesis and treatment of familial dysautonomia using patient-specific iPSCs. *Nature*, **461**, 402–406.
21. Ku, S., Soragni, E., Campau, E., Thomas, E.A., Altun, G., Laurent, L.C., Loring, J.F., Napierala, M. and Gottesfeld, J.M. (2010) Friedreich's ataxia induced pluripotent stem cells model intergenerational GAA TTC triplet repeat instability. *Cell Stem Cell*, **7**, 631–637.
22. Chamberlain, S.J., Chen, P.F., Ng, K.Y., Bourgois-Rocha, F., Lemtiri-Chlieh, F., Levine, E.S. and Lalande, M. (2010) Induced pluripotent stem cell models of the genomic imprinting disorders Angelman and Prader-Willi syndromes. *Proc. Natl Acad. Sci. USA*, **107**, 17668–17673.
23. Nguyen, H.N., Byers, B., Cord, B., Shcheglovitov, A., Byrne, J., Gujar, P., Kee, K., Schüle, B., Dolmetsch, R.E., Langston, W. *et al.* (2011) LRRK2 mutant iPSC-derived DA neurons demonstrate increased susceptibility to oxidative stress. *Cell Stem Cell*, **8**, 267–280.
24. Marchetto, M.C., Carromeu, C., Acab, A., Yu, D., Yeo, G.W., Mu, Y., Chen, G., Gage, F.H. and Muotri, A.R. (2010) A model for neural development and treatment of Rett syndrome using human induced pluripotent stem cells. *Cell*, **143**, 527–539.
25. Okada, Y., Matsumoto, A., Shimazaki, T., Enoki, R., Koizumi, A., Ishii, S., Itoyama, Y., Sobue, G. and Okano, H. (2008) Spatiotemporal recapitulation of central nervous system development by murine embryonic stem cell-derived neural stem/progenitor cells. *Stem Cells*, **26**, 3086–3098.
26. Miura, K., Okada, Y., Aoi, T., Okada, A., Takahashi, K., Okita, K., Nakagawa, M., Koyanagi, M., Tanabe, K., Ohnuki, M. *et al.* (2009)

Variation in the safety of induced pluripotent stem cell lines. *Nat. Biotechnol.*, **27**, 743–745.
27. Beher, D., Wrigley, J.D., Nadin, A., Evin, G., Masters, C.L., Harrison, T., Castro, J.L. and Shearman, M.S. (2001) Pharmacological knock-down of the presenilin 1 heterodimer by a novel gamma-secretase inhibitor: implications for presenilin biology. *J. Biol. Chem.*, **276**, 45394–45402.
28. Okochi, M., Fukumori, A., Jiang, J., Itoh, N., Kimura, R., Steiner, H., Haass, C., Tagami, S. and Takeda, M. (2006) Secretion of the Notch-1 Abeta-like peptide during Notch signaling. *J. Biol. Chem.*, **281**, 7890–7898.
29. Zhou, S., Zhou, H., Walian, P.J. and Jap, B.K. (2005) CD147 is a regulatory subunit of the gamma-secretase complex in Alzheimer's disease amyloid beta-peptide production. *Proc. Natl Acad. Sci. USA*, **102**, 7499–7504.
30. He, G., Luo, W., Li, P., Remmers, C., Netzer, W.J., Hendrick, J., Bettayeb, K., Flajolet, M., Gorelick, F., Wennogle, L.P. *et al.* (2010) Gamma-secretase activating protein is a therapeutic target for Alzheimer's disease. *Nature*, **467**, 95–98.
31. Kyriazis, G.A., Wei, Z., Vandermey, M., Jo, D.G., Xin, O., Mattson, M.P. and Chan, S.L. (2008) Numb endocytic adapter proteins regulate the transport and processing of the amyloid precursor protein in an isoform-dependent manner: implications for Alzheimer disease pathogenesis. *J. Biol. Chem.*, **283**, 25492–25502.
32. Liu, G.H., Barkho, B.Z., Ruiz, S., Diep, D., Qu, J., Yang, S.L., Panopoulos, A.D., Suzuki, K., Kurian, L., Walsh, C. *et al.* (2011) Recapitulation of premature ageing with iPSCs from Hutchinson–Gilford progeria syndrome. *Nature*, **472**, 221–225.
33. Zhang, J., Lian, Q., Zhu, G., Zhou, F., Sui, L., Tan, C., Mutalif, R.A., Navasankari, R., Zhang, Y., Tse, H.F. *et al.* (2011) A human iPSC model of Hutchinson Gilford progeria reveals vascular smooth muscle and mesenchymal stem cell defects. *Cell Stem Cell*, **8**, 31–45.
34. Yazawa, M., Hsueh, B., Jia, X., Pasca, A.M., Bernstein, J.A., Hallmayer, J. and Dolmetsch, R.E. (2011) Using induced pluripotent stem cells to investigate cardiac phenotypes in Timothy syndrome. *Nature*, **471**, 230–234.
35. Carvajal-Vergara, X., Sevilla, A., D'Souza, S.L., Ang, Y.S., Schaniel, C., Lee, D.F., Yang, L., Kaplan, A.D., Adler, E.D., Rozov, R. *et al.* (2010) Patient-specific induced pluripotent stem-cell-derived models of LEOPARD syndrome. *Nature*, **465**, 808–812.
36. Mattis, V.B. and Svendsen, C.N. (2011) Induced pluripotent stem cells: a new revolution for clinical neurology? *Lancet Neurol.*, **10**, 383–394.
37. Hu, B.Y., Weick, J.P., Yu, J., Ma, L.X., Zhang, X.Q., Thomson, J.A. and Zhang, S.C. (2010) Neural differentiation of human induced pluripotent stem cells follows developmental principles but with variable potency. *Proc. Natl Acad. Sci. USA*, **107**, 4335–5340.
38. Boulting, G.L., Kiskinis, E., Croft, G.F., Amoroso, M.W., Oakley, D.H., Wainger, B.J., Williams, D.J., Kahler, D.J., Yamaki, M., Davidow, L. *et al.* (2011) A functionally characterized test set of human induced pluripotent stem cells. *Nat. Biotechnol.*, **29**, 279–286.
39. Busciglio, J., Lorenzo, A., Yeh, J. and Yankner, B.A. (1995) Beta-amyloid fibrils induce tau phosphorylation and loss of microtubule binding. *Neuron*, **14**, 879–888.
40. Jin, M., Shepardson, N., Yang, T., Chen, G., Walsh, D. and Selkoe, D.J. (2011) Soluble amyloid β-protein dimers isolated from Alzheimer cortex directly induce Tau hyperphosphorylation and neuritic degeneration. *Proc. Natl Acad. Sci. USA*, **108**, 5819–5824.
41. Bierer, L.M., Hof, P.R., Purohit, D.P., Carlin, L., Schmeidler, J., Davis, K.L. and Perl, D.P. (1995) Neocortical neurofibrillary tangles correlate with dementia severity in Alzheimer's disease. *Arch. Neurol.*, **52**, 81–88.
42. Schmitt, O., Eggers, R. and Haug, H. (1995) Quantitative investigations into the histostructural nature of the human putamen. I. Staining, cell classification and morphometry. *Ann. Anat.*, **177**, 243–250.
43. Jiang, Q., Lee, C.Y., Mandrekar, S., Wilkinson, B., Cramer, P., Zelcer, N., Mann, K., Lamb, B., Willson, T.M., Collins, J.L. *et al.* (2008) ApoE promotes the proteolytic degradation of Abeta. *Neuron*, **58**, 681–693.
44. Mawuenyega, K.G., Sigurdson, W., Ovod, V., Munsell, L., Kasten, T., Morris, J.C., Yarasheski, K.E. and Bateman, R.J. (2010) Decreased clearance of CNS beta-amyloid in Alzheimer's disease. *Science*, **330**, 1774.